Scientific Reports

https://doi.org/10.1038/s41598-026-43056-z

Article in Press

Research on deformation mechanisms in deep excavation tunnels and the application of the pile foundation-unit-type support

Received: 8 November 2025

Accepted: 28 February 2026

Published online: 09 March 2026

Cite this article as: Gou L., An D., Song Y. *et al.* Research on deformation mechanisms in deep excavation tunnels and the application of the pile foundation-unit-type support. *Sci Rep* (2026). https://doi.org/10.1038/s41598-026-43056-z

Leiyu Gou, Dong An, Yimin Song, Hailiang Xu, Wujian Xiao & Xiaodong Jiang

Research on deformation mechanisms in deep excavation tunnels and the application of the pile foundation-unit-type support

Leiyu Gou[1], Dong An [1,*], Yimin Song [1], Hailiang Xu [1], Wujian Xiao [1], Xiaodong Jiang [1]

[1]North China University of Technology, Beijing 100114.
*Correspondence: andong@ncut.edu.cn (Dong An).

Abstract : To address post-excavation deformation and failure in deep underground mine tunnels, this study investigates the auxiliary transport tunnel in the northern wing of the 3-1 coal seam at a coal mine in Inner Mongolia. Field structural sampling, laboratory testing, and in situ measurements were conducted to determine the rock mass structure, lithological parameters, and stress distribution in the tunnel roof and floor. A numerical model of the surrounding rock and an analytical model of tunnel floor displacement were developed to analyze the failure mechanism of the tunnel. A support scheme combining pile–foundation unit-type support with anchor bolts and cables is proposed to control tunnel deformation. The effectiveness of this synergistic support scheme was validated through numerical simulation. The research indicates that excavation redistributes the in-situ stress, generating zones of tensile stress and areas of high compressive stress concentration both around the tunnel and deep within the surrounding rock. This leads to the development of both tensile and compressive plastic zones within the surrounding rock, leading to deformation and failure of the rock-tunnel interface. The magnitude of roadway floor displacement is proportional to both the width of the plastic zones at the floor ends and the stress concentration factors on each side. The point of maximum floor displacement shifts toward the side with the wider plastic zone or the higher stress concentration factor. Under the combined support system, the maximum displacements of the roof and floor were reduced by 93% and 82%, respectively, while the maximum deformation values for the roadway sides decrease by 78% and 93%, respectively. The displacement patterns of the roof and floor were significantly improved, with the plastic strain zone in the surrounding rock completely severed and the maximum plastic strain value reduced by approximately 80%. Therefore, effective control of tunnel deformation relies on enhancing the integrity of the surrounding rock and reducing both stress concentration and plastic flow. The synergistic effect of the pile-foundation unit support with the anchor bolts and cables effectively mitigated post-excavation deformations, including floor heave, roof settlement, and sidewall convergence, demonstrating the effectiveness and feasibility of the proposed synergistic support scheme for mitigating tunnel deformation.

Keywords : Tunnel deformation; stress concentration; plastic flow; tunnel support

0 Introduction

As critical underground passages, tunnel play essential roles in ventilation, personnel access, and material transportation[1]. During excavation, factors such as geological structures, high in situ stress, and weak surrounding rock often lead to deformation and failure[2], which severely

compromise mine safety and productivity. Therefore, analyzing roadway deformation mechanisms and developing effective control measures is of great engineering significance for safe mining operations.

In recent years, significant progress has been made in researching and mitigating the failure of tunnel roof[3, 4], floor[5, 6], and sidewalls[7, 8]. Kang[9, 10] identified rock expansion, buckling, and rheological behavior as key causes of tunnel floor heaving, proposing that reducing floor stress and enhancing rock stability are effective preventive measures. Xia[11] suggest that excessive coal face space without horizontal constraints accelerates coal face failure and rib spalling, subsequently triggering roof falls. Li[12] proposed controlling the depth of rib caving and preventing roof falls through methods such as enhancing support by improving roof supports, reducing coal face deflection, and improving coal body integrity via chemical grouting. Numerous scholars have proposed diverse support schemes and research methodologies. Zhao[13] employed field measurements, theoretical analysis, and numerical simulation to determine that the primary cause of roadway failure lies in the tensile and compressive stress field resulting from the combined effects of advance support pressure at the working face and stress concentration in residual coal pillars. He further optimized the roadway bolt and cable support systems. Deng[14] utilized the Flac^{3D} numerical model to elucidate the deformation mechanism of bulging in large-section soft rock inclined shafts. He proposed an optimized support scheme combining "reverse bottom arch + cable anchors." Su[15] investigated the failure mechanisms of the rib, shoulder, and roof in lower coal seam roadways through theoretical calculations. He proposed an optimized solution to enhance roadway deformation control by strengthening anchor rod and cable support and improving roadway cross-section design. The feasibility of this solution was verified through numerical simulation. Song[16] proposed pile-supported hydraulic portal roof supports to prevent bottom bulging, verifying the support performance through numerical simulation and similarity testing.

Existing approaches primarily focus on enhancing the overall strength of the surrounding rock through bolts and cables[17] and alleviating stress concentration by relieving pressure [18]. These approaches provide theoretical guidance for preventing roadway floor bulging and roof/sidewall failures, while also demonstrating the feasibility of numerical simulation and theoretical analysis in studying roadway failure mechanisms and the performance of support schemes[19, 20]. During the excavation of the North Wing auxiliary transport tunnel in the 3-1 coal seam of a coal mine in Inner Mongolia, problems such as floor heave, roof subsidence, and rib deformation occurred, resulting in floor cracking and compromising vehicular safety, despite the existing bolt and cable support system. To investigate the deformation mechanism, structural sampling, processing tests, and stress detection were conducted on the rock strata. A numerical model of the deep underground roadway surrounding rock and a mechanical theoretical model of the floor bulging were established.Based on the concept of preventing tunnel deformation by enhancing rock mass integrity, strengthening support strength, and improving rock stress conditions, this study proposes a pile foundation-unit-type support system integrating the advantages of modular hydraulic anti-shock supports[21]. This system, in combination with the existing rock bolts and cables, forms a synergistic support scheme, and the feasibility of this synergistic support scheme is investigated through numerical simulation.

1. Basic conditions of the tunnel and surrounding rock

1.1 Deformation of the surrounding rock in the tunnel

The coal mine in Inner Mongolia is located on the northern Ordos Plateau. The site features a monoclinal structure with a general southwesterly dip, with a dip direction of 200–230° and a stratigraphic dip angle less than 5°. Local areas show broad, gentle undulations, with no significant folds or faults identified and no evidence of magmatic activity. The primary mining target is the 3-1 coal seam, buried at a depth of approximately 420 meters. Exploration reports indicate a natural coal seam thickness ranging from 2.70 to 6.85 meters, averaging 5.31 meters. The coal seam is stable in occurrence, well developed across the entire area, and economically minable. Three north-south roadways are arranged in the central section of the coal mine: a belt conveyor roadway, an auxiliary transport roadway, and a return airway. During mine development, displacement deformation occurred in the 3-1 North Wing Auxiliary Transport Tunnel. The most severe deformation manifested as floor heave, characterized by pronounced asymmetric uplift near the solid coal side. This caused floor cracking, compromising vehicle safety. The rib on the coal pillar side experienced the second-most severe damage, manifesting as localized bulging that displaced the support plates. Deformation of the roof and the solid coal rib was relatively minor.

Figure 1. Tunnel deformation conditions

1.2 Stratigraphic structure and parameters

Sampling and analysis were conducted on the roof and floor strata within the North Wing Auxiliary Transport Tunnel of the 3-1 coal seam. The drill hole was located in the No. 2 reversing chamber of the northern wing auxiliary transport drift in the second panel area of the 3-1 coal seam. The extracted core samples are shown in Figure 2. Based on the core sampling results and local geological conditions of the coal mine, the characteristics of the coal seam and overlying/underlying strata within the North Wing Auxiliary Transport Tunnel of the 3-1 coal seam are summarized in Table 1.

a.Drilling **b.Core extraction** **c.Conglomerate** **d.Fine sandstone** **e.Sandy mudstone**

Figure 2. On-site rock coring operations

Table 1. Coal seam and roof/floor strata conditions in the North Wing Auxiliary Transport Tunnel

Lithology	Rock layer thickness（m）	Characteristics of coal seam formation

Conglomerate(R3)	17.14	Light gray, composed primarily of quartzite and feldsparite, poorly sorted, with clayey interstices.
Fine sandstone(R2)	8.68	Grayish white, dominated by quartz and feldspar, poorly sorted, mud-cemented, with thin mudstone interbeds; sandstone grain size and cementation gradually decrease from bottom to top.
Sandy mudstone(R1)	4.14	Dark gray, sandy-clayey texture, nearly horizontal bedding, flat-looking fracture surfaces, abundant fossilized plant stems, intact core, semi-hard
3-1 Coal	5.94	Black, with a weak bituminous sheen, containing thread-like carbon, predominantly dark coal, semi-dark type.
Sandstone interbedded with siltstone(F1)	33.13	Dark gray, sandy-clayey texture, with a flat fracture surface, containing a small amount of fossilized plant leaves and stems.

The rock and coal samples collected on-site undergo secondary processing at a specialized facility to produce standard cylindrical specimens approximately 100 mm in height and 50 mm in diameter. These processed specimens are subjected to uniaxial compression tests, triaxial compression tests, and Brazilian splitting tests as shown in Figure 3, yielding relevant physical and mechanical property parameters.

a.Uniaxial compression test **b.Triaxial compression test** **c.Brazilian split test**

Figure3. Rock property testing

Table 2. Test results of physical and mechanical parameters of coal seam and overlying/underlying rock masses

Lithology	Density kg/m³	Modulus of elasticity GPa	Poisson ratio	Cohesion MPa	Internal friction angle °	Expansion angle °	Tensile strength MPa
Conglomerate(R3)	2430	5.32	0.23	3.32	42	19	1.05
Fine sandstone(R2)	2202	3.10	0.33	3.20	30	21	0.62
Sandy mudstone(R1)	2290	2.92	0.32	2.56	29	16	1.31
3-1 Coal	1500	1.59	0.34	4.23	29	16	0.61
Sandstone interbedded with siltstone(F1)	2328	4.91	0.31	3.96	34	16	1.10

To determine the in-situ rock stress conditions of the coal mine, six measurement points were selected within the exposed range of existing roadways for in-situ rock stress testing. The in-situ stress test results indicate: For the 3-1 coal seam, the maximum principal stress in the in-situ rock stress field is horizontal stress, with a magnitude ranging from 15.72 to 17.94 MPa and a direction between 55.02º and 65.49º; The maximum horizontal principal stress exceeded the vertical stress, being 1.44 to 1.57 times greater than the vertical stress. This disparity will influence the deformation and failure patterns of underground rock strata as well as the manifestation of rock pressure. The measured maximum horizontal principal stress was 1.81 to 1.91 times the minimum

horizontal principal stress. The measured vertical stress was essentially consistent with the vertical stress calculated based on the thickness and unit weight of the overlying strata.

1.3 Existing roadway support

The cross-sectional dimensions of the North Wing Auxiliary Transport Tunnel are 5.4m × 3.8m. One side is solid coal, while the other side is a 7.2m coal pillar. The existing support consists of anchor bolts and anchor cables. Anchor rod and cable material dimensions are detailed in Table 3. Anchor rods are φ22mm diameter, 2600mm long threaded steel fine-thread anchor rods; anchor cables are φ21.8mm diameter, 7300mm long mining anchor cables. The anchor rod rows are spaced at 1000 mm intervals, while the anchor cable rows are spaced at 2000 mm intervals. The specific layout is shown in Figure 4.

Table 3. Anchor bolt and cable parameters

	Diameter mm	Length mm	Row spacing mm	Density kg/m^3	Poisson ratio	Young's modulus GPa	Yield stress MPa	Tensile strength MPa
Anchor rod	22	2600	1000	7960	0.3	210	700	630
Anchor cable	21.8	7300	2000	7850	0.3	200	700	1770

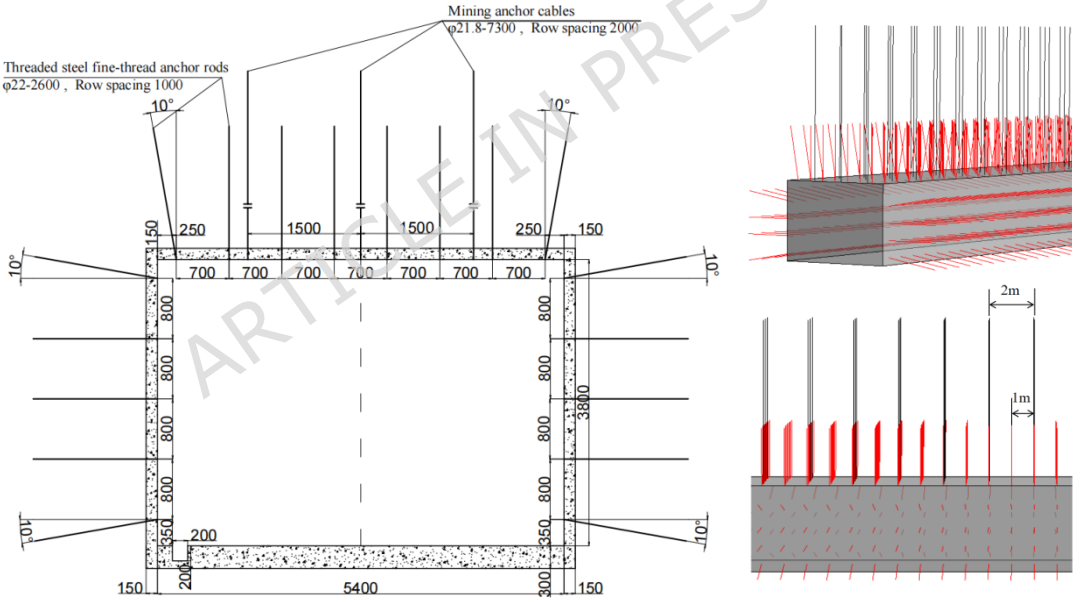

Figure 4. Schematic diagram of cross-section shape and anchor bolt/cable arrangement for North Wing Auxiliary Transport Tunnel

2 Analysis of causes of tunnel deformation

2.1 Numerical computation model

To investigate the deformation and failure mechanisms of mine tunnels, a numerical simulation model of the surrounding rock was established using ABAQUS numerical analysis software to simulate the stress state at great depths underground. The rock mass in the model employs an elastic-plastic constitutive relationship with Mohr-Coulomb yield criteria, disregarding material softening and damage evolution. The physical and mechanical parameters of

coal and rock strata are listed in Table 2. In the spatial coordinate system, the horizontal lateral direction is the *x*-axis, the vertical direction is the *y*-axis, and the horizontal direction perpendicular to the paper surface is the *z*-axis. The model dimensions were 63.8m × 42.6m × 72m. The bottom boundary was fully fixed, and displacement in the *z*-direction at the front and rear boundaries was constrained to approximate a plane-strain condition, consistent with a tunnel whose longitudinal extent greatly exceeds its cross-sectional dimensions. Based on the rock stress data obtained from testing, combined with rock density calculations, a uniformly distributed vertical pressure of 10 MPa was applied at the top to simulate overburden pressure, while a horizontal gradient pressure of 15–18 MPa was applied at the left and right boundaries to simulate lateral pressure. The pre-tension force for the anchor bolts (cables) in the model are set to 100 kN. An anchorage length of 300 mm is defined at the end of the anchor bolts (cables), while the other end is fixed to the tunnel rock surface. The entire anchor bolt and cable were modeled as being fully embedded in the surrounding rock.

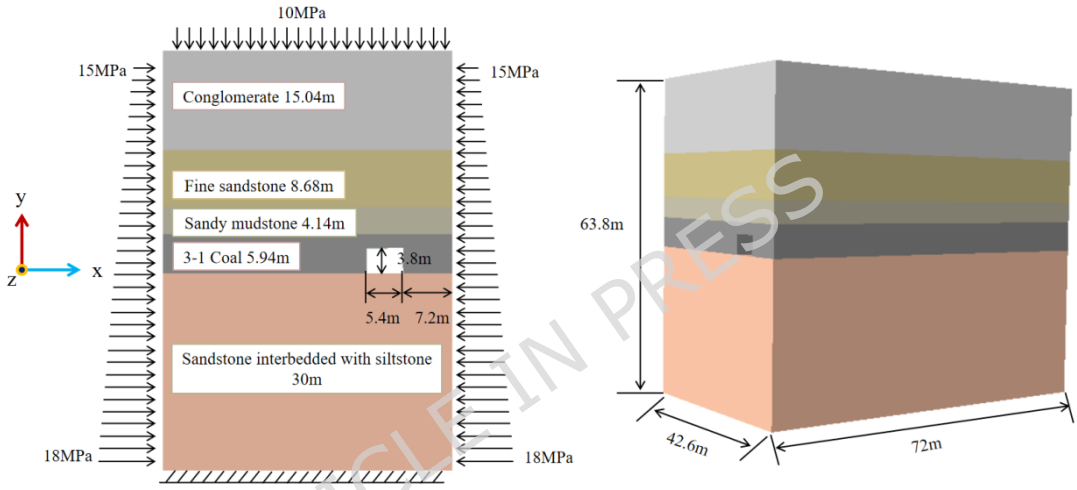

Figure 5.Bearing rock numerical model

The simulation results indicate that under in situ stress, the roadway exhibits pronounced irregular and asymmetric floor heave, along with deformation of the roof and sidewalls. As shown in the roadway displacement curve diagram, both the roadway roof and floor, as well as both sidewalls, have experienced displacement deformation compressing inward toward the roadway. The maximum floor bulging reached 514 mm, occurring on the left side of the floor. The maximum roof subsidence was 264 mm. The maximum horizontal displacements for the left rib (solid coal side) and right rib (coal pillar side) were 156 mm and 402 mm, respectively.

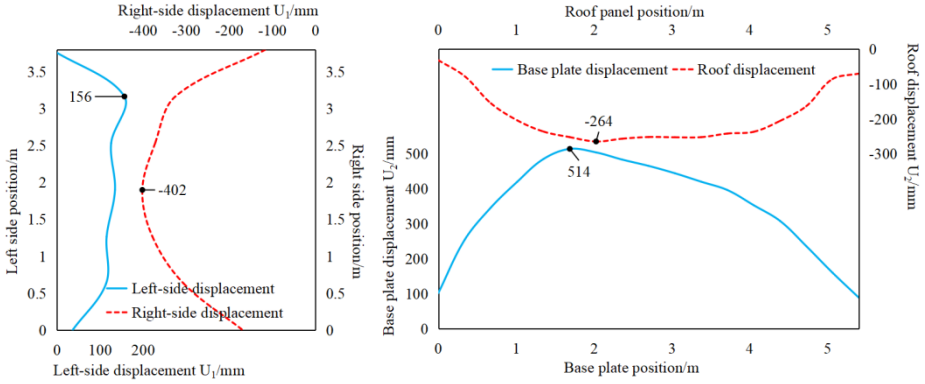

Figure 6.Displacement curve of roadway under anchor bolt and cable support

The plastic strain contour map reveals a nearly elliptical, ring-shaped continuous plastic zone

near the tunnel. Overall, the most severely damaged rock mass areas are located at the tunnel floor near the solid coal body and along the right tunnel wall (coal pillar side). This corresponds to the displacement deformation characteristics of the tunnel, where the maximum displacement positions roughly align with the high plastic strain zones in the roof and floor rock mass. From the PE11 cloud diagram, which represents horizontal strain, plastic elongation occurs at the tunnel sidewalls while compression zones appear at the roof and floor. The maximum plastic strains for tension and compression are 0.135 and 0.082, respectively. This indicates that horizontally, the tunnel sidewalls undergo tensile deformation while the roof and floor experience compressive deformation mechanisms. From the PE22 stress-strain diagram, tensile zones appear at the tunnel roof and floor, while compressive zones occur at the sidewalls. The maximum tensile and compressive plastic strains are 0.174 and 0.067, respectively. This indicates a deformation mechanism where the tunnel roof and floor undergo tensile deformation while the sidewalls experience compressive deformation in the vertical direction.

This occurs because tunnel excavation disturbs the original stress equilibrium within the rock mass, causing stresses to redistribute around the tunnel. Horizontal stress σ_{xx} and vertical stress σ_{yy} form high-stress concentration zones deep within the rock mass at the roof, floor, and both sides. Consequently, areas of varying degrees of tensile stress emerge at the tunnel's roof, floor, and sides, creating typical “compressive stress concentration” and “tensile stress zones.” Consequently, the high horizontal stress concentration deep within the rock mass compresses the sidewall rock, while the high vertical stress concentration compresses the roof and floor rock. Under the combined action of tensile stress, the rock mass undergoes plastic flow and shear failure, generating tensile fractures. This mechanism leads to floor heave, roof collapse, and sidewall extrusion. Furthermore, due to significant variations in coal thickness along the left and right walls and in rock layer parameters between the roof and floor, stress distributions across the walls, roof, and floor are asymmetrical. Consequently, the tunnel exhibits asymmetric and irregular deformation in its roof, floor, and walls.

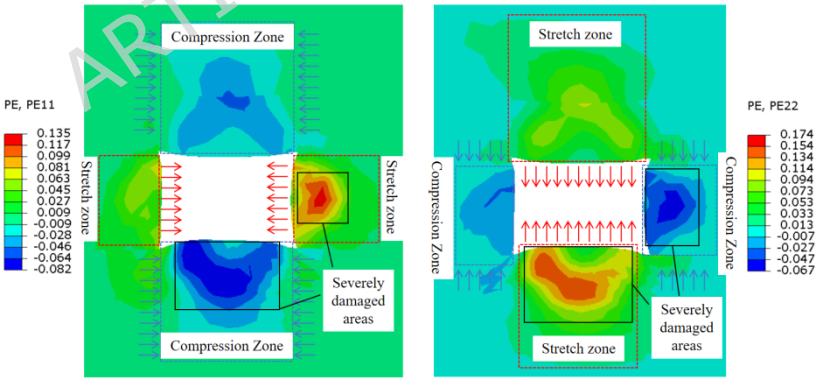

Figure 7. Plastic strain of tunnel surrounding rock under anchor bolt and cable support

2.2 Mechanical theory model of tunnel bottom bulging

The stress distribution in the roadway floor is linearized. The deformation of the roadway floor and the characteristics of the vertical stress distribution on the floor are shown in Figure 8. K and K' represent the stress concentration factors for the solid coal side and the coal pillar side, respectively; γ denotes the unit weight of the overlying rock mass; and H indicates the roadway burial depth. Under the combined pressure from both sides, the roadway floor gradually softens,

forming a plastic zone. The undamaged floor rock mass deep within the surrounding rock remains an elastic zone. When support pressure becomes excessive, it causes complete failure of the surrounding rock mass around the tunnel, leading to plastic flow toward the tunnel center and forming a bulge. Due to differing coal conditions on each side of the tunnel, the stress distribution is asymmetric, resulting in an uneven plastic strain zone. This manifests as a distinct asymmetric bulge on the floor, with the maximum bulge location occurring near the solid coal side.

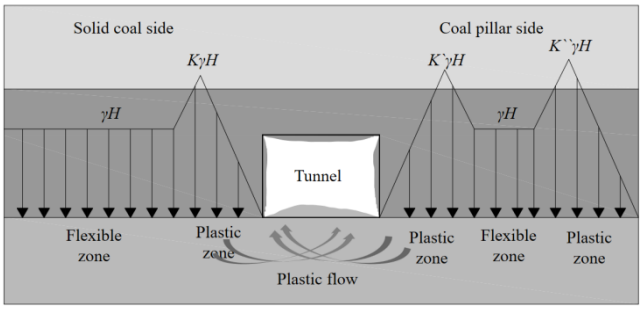

Figure 8. Characteristics of stress distribution in tunnel bottom drum and floor slab

To discuss the displacement behavior of the roadway floor bulge under theoretical conditions, the direct roadway floor is further simplified into a rectangular cross-section simply supported beam based on the stress distribution characteristics of the floor slab. A theoretical calculation model for the floor bulge is established as shown in the figure. Segment $AA`$ represents the roadway floor slab with a width of $x_0$; Sections $AB$ and $A`B`$ represent the solid coal side and coal pillar side plastic zones, respectively, with widths $x_1`$ and x_1. Vertical displacements at points A and $A`$ are fixed. Under limit conditions, shear forces and bending moments from the elastic zones on both sides to the plastic zones at the end plates are neglected, i.e., $F_B$, $M_B$, $F_B`$, and $M_B`$ at both ends are set to zero.N represents the equivalent vertical support reaction force provided by the strut and the two side rock masses to the floor slab; $\gamma H-N$ denotes the net vertical additional pressure exerted on the floor slab after accounting for the support reaction force.

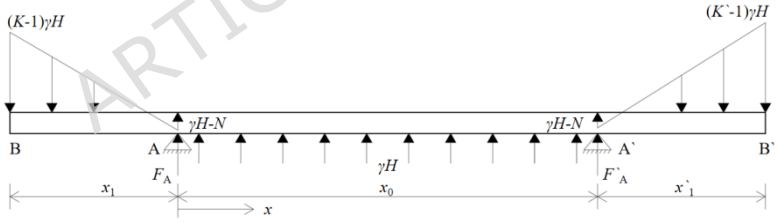

Figure 9. Mechanical model diagram of the base plate

According to the equilibrium of moments at point A,

$$\frac{1}{3}x_1^2(K\square H\square N)\square\frac{1}{2}x_1^2(\square H\square N)\square\frac{1}{2}x_0^2\square H\square x_0F_{A`}$$
$$\square(\frac{1}{3}x`_1^2\square\frac{1}{2}x`_1x_0)(K`\square H\square N)\square(\frac{1}{2}x_1^2\square x`_1x_0)(\square H\square N)\square0 \quad (1)$$

The vertical reaction force at point A' can be obtained

$$F_{A`}\square\frac{1}{6x_0}\left[\begin{array}{l}\square(2x`_1^2\square3x`_1x_0)(K`\square H\square N)\square2x_1^2(K\square H\square N)\square\\\square3(x_1^2\square x`_1^2\square2x`_1x_0)(\square H\square N)\square3x_0^2\square H\end{array}\right] \quad (2)$$

Similarly, the moment equilibrium at point $A`$,

$$(\frac{1}{3}x_1^2 - \frac{1}{2}x_1x_0)(K-H-N) - (\frac{1}{2}x_1^2 - x_1x_0)(-H-N) - x_0F_A + \frac{1}{2}x_0^2-H - \frac{1}{3}x_1^{`2}(K-H-N) - \frac{1}{2}x_1^{`2}(-H-N) = 0 \quad (3)$$

The vertical reaction force at point A can be obtained:

$$F_A = \frac{1}{6x_0}[(2x_1^2 - 3x_1x_0)(K\gamma(-N) - 2x_1^{`2}(K`\gamma K - N) - 3(x_1^{`2} - x_1^2 - 2x_1x_0)(\gamma(-N) - 3x_0^2\gamma H] \quad (4)$$

On the base plate, i.e., segment AA', the condition for torque equilibrium at any point x from point A is:

$$(\frac{1}{3}x_1^2 - \frac{1}{2}x_1x)(K-H-N) - (\frac{1}{2}x_1^2 - x_1x)(-H-N) - F_Ax + \frac{1}{2}x^2-H - M_x = 0 \quad (5)$$

Setting $a_1 = \frac{1}{2}-H$, $a_2 = x_1(-H\frac{1}{2}K-H\frac{1}{2}N) - F_A$, $a_3 = x_1^2(\frac{1}{2}-H\frac{1}{3}K-H\frac{1}{6}N)$ yields:

$$M_x = a_1x^2 + a_2x + a_3 \quad (6)$$

According to the displacement calculation formula for beams in the mechanics of materials, we have $M_x = EI\frac{d^2w}{dx^2}$, that is, $M_x = EIw''$. Therefore, equation (6) can be transformed into the differential equation for the deflection curve of the beam as follows,

$$EIw'' = a_1x^2 + a_2x + a_3 \quad (7)$$

In the equation, w represents the deflection of the simply supported beam, in m; E denotes the elastic modulus of the direct roadway base, in GPa; I signifies the moment of inertia of the beam's cross-section about the neutral axis, in m⁴. After performing double integration on the beam's deflection differential equation, we obtain,

$$w = \frac{1}{EI}(\frac{1}{12}a_1x^4 + \frac{1}{6}a_2x^3 + \frac{1}{2}a_3x^2 + a_4x + a_5) \quad (8)$$

Based on the boundary condition that the deflection of a simply supported beam is zero at the supports, namely points A and A', we have: $w = 0$ when $x = 0$, $w = 0$ when $x = 5.4$ m. From this, it can be calculated that, $a_5 = 0$, $a_4 = -\frac{1}{12}a_1 - \frac{1}{6}a_2 - \frac{1}{2}a_3$. Assuming the bottom plate beam cross-section has a unit width and the direct bottom thickness is approximately 3m, the deflection curve equation can be obtained as,

$$w = \frac{1}{E\cdot 3^3}(a_1x^4 + 2a_2x^3 + 6a_3x^2 + 12a_4x) \quad (9)$$

In the equation, let x represent the variable value and w represent the function value. Set the stress concentration factors K and $K`$ for the solid coal side and coal pillar side to 1.5, respectively. The width $x_1`$ of the plastic zone on the coal pillar side of the floor is 3m, while the width x_1 of the plastic zone on the solid coal side is varied from 3m to 8m. Set the widths of the plastic zones on both sides of the floor x_1 and $x_1`$ to 3 m, the stress concentration factor $K`$ on the pillar side to 1.5, and the stress concentration factor K on the solid coal side from 1.5 to 4. Calculate the deflection curves of the roadway floor beams under different floor plastic zone widths and stress concentration factors, i.e., the displacement curves of the roadway floor, as shown in Figure 10. It

can be observed that when the plastic zone widths on both sides of the floor and the stress concentration factor on the solid coal side are identical, the maximum displacement point occurs at the center of the floor. However, as the plastic zone width x_1 on the solid coal side and the stress concentration factor K on the solid coal side increase, the displacement magnitude significantly rises, and the location of the maximum displacement gradually shifts toward the solid coal side. It can be concluded that the width of the plastic zone in the roadway floor and the stress concentration factor on the rib side are key factors determining roadway floor heave. The maximum heave occurs closer to the side with a larger plastic zone width and stress concentration factor. Therefore, when factors such as roadway burial depth, overburden unit weight, direct floor thickness, and floor elastic modulus are difficult to alter, floor heave can be controlled by reducing the width of the plastic zone and the stress concentration factor on the rib side.

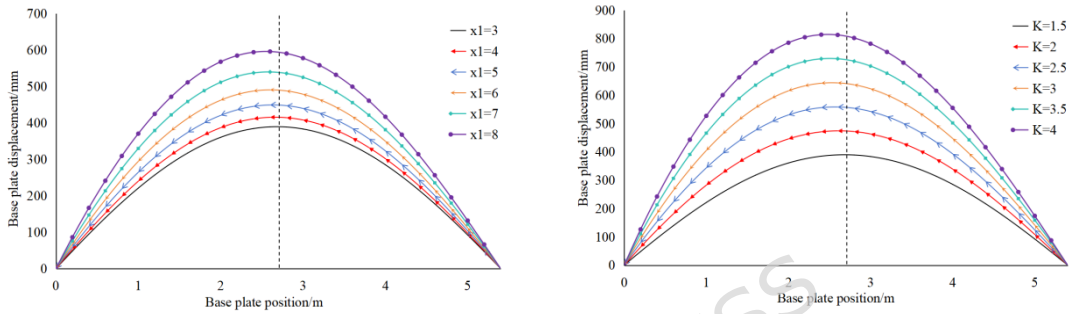

a.Displacement curve of tunnel floor when x_1 varies **b.Displacement curve of tunnel floor when K varies**

Figure 10. Displacement curve of the tunnel floor

3 Application of the pile foundation-unit-type support in mitigating tunnel damage

Given that the current anchor rod and cable support system has not effectively controlled tunnel deformation, and to prevent subsequent disturbances or impacts from disrupting the tunnel's equilibrium and causing further damage, it is necessary to reinforce the tunnel support system. The guiding principle for this reinforcement should focus on improving the plastic zone at the tunnel floor and reducing stress concentration at the sidewalls.

3.1 Proposed the pile foundation-unit-type support

Traditional unit-type anti-collapse energy-absorbing supports[21] feature robust support performance, excellent synergy with surrounding rock, and strong fatigue resistance. They are key equipment specifically designed for deep mining operations. Although current design concepts emphasize “lightweight” and “self-moving” features, complex issues such as floor cracking caused by unevenness due to heaving in underground roadways mean that traditional unit props still face problems like tilting and difficulty in moving. Therefore, based on the design philosophy of the pile foundation control base drum from the research team's existing hydraulic support for pile foundation[16] and pile foundation-three-hinge arch support[22], a pile foundation-unit-type support is proposed. Using the bored pile method, the pile body is driven into the roadway floor in advance and the pile cap is secured. At the required support unit spacing intervals, modular supports are fixed to the pile cap at suitable locations, forming the pile foundation-unit-type support. On one hand, the piles driven into the floor rock mass improve the stress environment of the floor rock mass, enhance its stability, and improve the plastic zone of the roadway floor,

thereby controlling roadway floor displacement; On the other hand, the leveling of the cap allows for more stable and vertical placement of supports, enabling them to better align with their working force lines. This enhances the support performance of modular anti-impact energy-absorbing supports, thereby distributing and reducing stress concentration on the tunnel walls. Alternatively, tracks can be installed on the cap to facilitate easier movement of the supports.

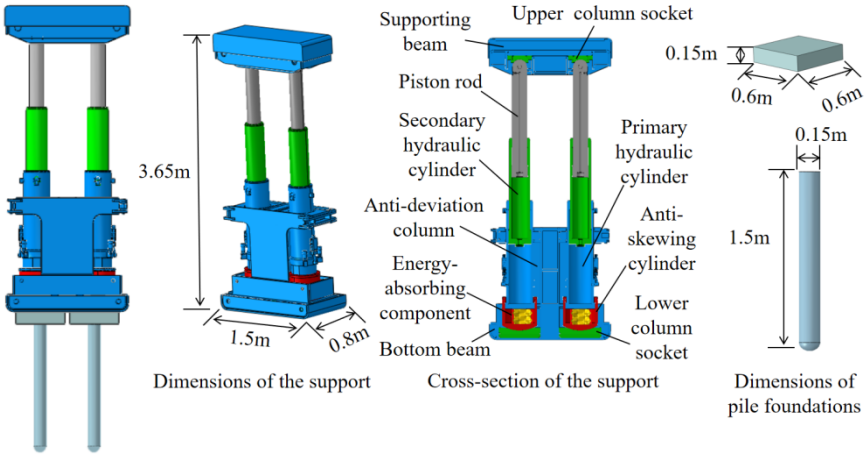

Figure 11. The pile foundation-unit-type support

Table 4 . Material Parameters for the pile foundation-unit-type support

	Thickness mm	Poisson ratio	Young's modulus GPa	Yield stress MPa	Density kg/m³
Supporting beam, Upper column socket	100	0.3	206	785	7850
Bottom beam	28.5				
Lower column socket, Anti-deviation column, Anti-skewing cylinder	25	0.3	206	835	
Piston rod	40				
Hydraulic cylinder	30.5				
Energy-absorbing component	8	0.26	210	785	
Pile cap	150	0.26	210	800	
Pile	——				

The dimensions and construction of the support frame and pile foundation are shown in the Figure 11. Both the support frame and pile foundation are made of high-strength steel. The various components of the support frame and the cap consist of steel plates of varying thicknesses. The pile consists of a steel column 150 mm in diameter and 1.5 m in length. Material parameters are listed in the table. The pile body and cap are welded together for fixation. with the pile fully driven into the roadway floor slab. The base of the cap rests flush against the roadway floor slab, and the support is vertically positioned atop the cap. Under ideal conditions, the working resistance of the support acts in the vertical direction, with no horizontal forces or bending moments between the support and the cap. Therefore, excessive fixation of the support and cap is

unnecessary. Simple clamps can be used to secure the support to the cap and prevent displacement due to rock mass vibrations.

3.2 Analysis of the support performance of the pile foundation-unit-type support

As shown in Figure 12, the pile foundation-unit-type support are added to the existing anchor rod and cable support system in the tunnel. Piles are arranged in two rows along the tunnel axis at symmetrical intervals of 3.6 meters, with 0.6 meters between each pile in a row. Supports are vertically installed at 3.6-meter intervals to form support units. The pile foundation-unit-type support and the rock bolts/cables form a synergistic support system. The confining pressure and boundary conditions remain unchanged from the previous section, and a numerical model of the surrounding rock under synergistic support is established.

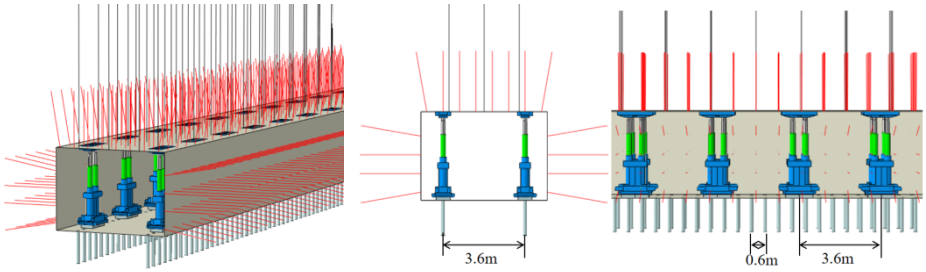

Figure 12. Schematic diagram of coordinated support arrangement for roadways

Numerical simulations indicate that under combined support, the maximum displacements of the roof and floor plates are 18 mm and 90 mm, respectively, while the maximum horizontal displacements of the left and right side walls are 35 mm and 29 mm, respectively. Compared to support using only rock bolts and cables, the maximum roof and floor plate displacements decrease by 93% and 82%, respectively, while the maximum side wall displacements decrease by 78% and 93%, respectively. Before the tunnel supports were installed, the displacement profiles of the tunnel roof and floor resembled "U" or "inverted U" curves. After installing the pile foundation-unit-type support within the tunnel, the displacement curves of the roof and floor exhibited significant changes. At locations corresponding to the pile rows and supports, displacement values showed a marked reduction. Under the synergistic support system, the maximum horizontal tensile and compressive plastic strains of the tunnel surrounding rock reached 0.046 and 0.013 respectively, representing reductions of 66% and 84% compared to the original values. The maximum vertical tensile and compressive plastic strains reached 0.031 and 0.010 respectively, showing decreases of 82% and 85% compared to the original values. Following the implementation of the synergistic support system, the plastic zone of the surrounding rock exhibited a "butterfly-shaped" configuration. The previously continuous annular plastic zone was distinctly fragmented, with the plastic strain zone at the tunnel floor being markedly isolated at the pile row locations.

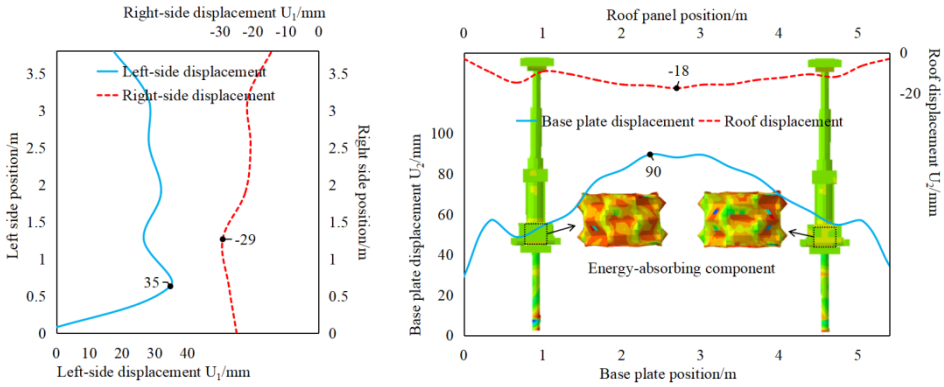

Figure 13. Tunnel displacement curve under collaborative support

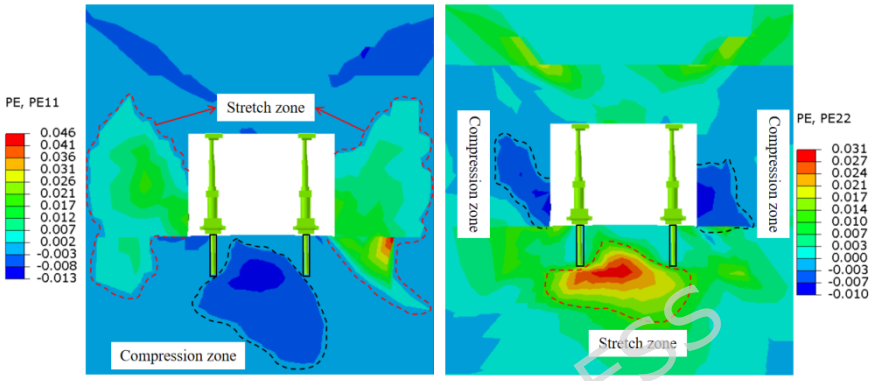

Figure 14. Plastic strain of tunnel surrounding rock under collaborative support

After installing the support, the high stress concentration near the tunnel was further alleviated. Deep within the roof and floor strata, intense stress concentration was mitigated, resulting in a more uniform stress distribution throughout the surrounding rock. High values of compressive and tensile stress concentrations were observed at the base of the pile rows and their vicinity. It can be concluded that the presence of the pile rows restrained the movement of the bedrock layer beneath the foundation slab, while the compression exerted by the bedrock layer induced high stress values within the pile bodies. It can be concluded that under the synergistic support effect, the row piles effectively blocked plastic strain in the floor, improved stress distribution within the surrounding rock, and enhanced the overall strength of the rock mass. The supports provided excellent structural reinforcement within the tunnel, alleviating stress concentration at both sides and controlling tunnel displacement to the “centimeter level.” This approach successfully suppressed tunnel deformation and failure to a significant degree. No stress concentration occurred at the connection points between the pile foundation and the support structure. The working resistance was transmitted vertically downward in alignment with the working force lines of both the pile foundation and the support structure. The connection between the support structure and the pile foundation was sound. The energy-absorbing devices of the support structure exhibited slight displacement, while the vertical columns of the support structure remained intact without failure. The support structure continues to function effectively in energy absorption and impact prevention.

4. Conclusions

(1) By establishing a numerical model of the tunnel surrounding rock, the deep underground confining pressure conditions in the auxiliary transport tunnel of the northern wing of the 3-1 coal seam in the coal mine were simulated. The investigation revealed that significant and extensive

deformation in the roof, floor, and both sidewalls of the roadway resulted from the redistribution of in-situ stresses during excavation. This redistribution caused high stress concentrations deep within the surrounding rock, compressing the surrounding rock mass around the roadway. Consequently, tensile stresses developed around the roadway, leading to plastic deformation and shear failure of the rock mass.

(2) Analysis of the mechanical theory model reveals that roadway bulging is influenced by multiple factors including roadway burial depth, overburden unit weight, direct base thickness, as well as floor width and elastic modulus. Asymmetric distribution of plastic zone width at both ends of the roadway floor and stress concentration factors on either side leads to asymmetric roadway bulging. Wider plastic zones and stronger stress concentration result in greater bulging deformation, with the peak position shifting toward that side.

(3) A pile-supported modular support system was proposed to prevent roof bulging, forming a synergistic support scheme with existing bolts (cables). Numerical results indicate that this synergistic support scheme significantly reduces roadway deformation and alters failure patterns. Compared to bolt (cable) support alone, roof displacement decreased by approximately 93% and floor bulging by approximately 82%. The sidewall displacements reduced by approximately 78% and 93%, respectively. The rock mass plastic zone, originally a continuous annular area, was distinctly fragmented into a “butterfly-shaped” configuration. The plastic zone in the floor was markedly interrupted at pile locations, with maximum plastic strain decreasing by 66%-85%. Furthermore, the supports remained intact without failure, continuing to function as energy-absorbing and impact-resistant supports, thereby validating the feasibility of the synergistic support scheme.

Availability of Data and Materials

All data generated or analysed during this study are included in this published article.

References

1. LIHUI S, BENSHENG Y, CHUNDONG S, et al. Experimental research on mechanism and controlling of floor heave in deep soft rock roadway. *J. Journal of Mining & Safety Engineering*, 2017, 34(02): 235-242.
2. ZIWEI D, SHUAI L, JIE Z, et al. Asymmetric failure mechanism and control of entries inshort-distance coal seam. *J. Journal of Mining & Safety Engineering*, 2024, 41(02): 242-254.
3. LI J, ZHOU W, DENG P, et al. Evolution of the roof caving and fracture zones during mining of close range coal seams. *J. Scientific Reports*, 2025, 15(1): 31221.
4. FEI L, DEZHONG K, QIANG L, et al. Failure analysis and prediction of roof instability in end face under repeated mining using early warning system. *J. Scientific reports*, 2023, 13(1): 8764.
5. YAODONG J, SHILIANG L. Research on the mechanism of bottom bulging in roadways. *J. Journal of China Coal Science*, 1994, (04): 343-351.
6. XU Q, LI X H, XIA Z, et al. Mechanism and control of floor heave in two entry retained roadways using dense boreholes. *J. Scientific Reports*, 2025, 15(1): 17243.
7. XUE B, SHANG Y, WANG C, et al. Research on bending-slip rib spalling and rib stability of extra-thick hard coal wall. *J. Scientific Reports*, 2025, 15(1): 26796.

8. ZHAO J, WANG X, BAI J, et al. Study on instability mechanisms and control of coal pillar spalling and coal crumbs leakage during working face crossing faults. *J. Scientific Reports*, 2024, 14(1): 26667.
9. HONGPU K, SHILIANG L. Analysis of the mechanism of roadway floor bulging. *J. China Journal of Rock Mechanics and Engineering*, 1991, (04): 362-373.
10. HONGPU K. The mechanism and prevention of floor bulging in soft rock roadways. *M. Beijing: Coal Industry Publishing House*, 1993: 1-3.
11. YONGXUE X, LIJUN K, QINGXIN Q. Coal cutting height affected to stability of coal wall in fully mechanized top coal cavingmining face with high coal cutting height. *J. Coal science and Technology*, 2008, 36(12): 1-3+21.
12. YAJUN L. Prevention technology of coal-wall slide and roof fall in large-mining height mining face. *J. Coal Mining Technology*, 2014, 19(04): 106-107+99.
13. HONGBAO Z, HU C, DONGLIANG J, et al. Study of the mechanism and evolution law of unsymmetricalfailure of the mining roadway in close distance coal seam. *J. Journal of China University of Mining & Technology*, 2021, 50(06): 1029-1040+50.
14. ZHUOYUE D, LIU OINJIE, TANG, et al. Mechanism and prevention of bottom heave in large cross-sectionInclined shaft roadways in swelling soft rocks. *J. Science Technology and Engineering*, 2025, 25(11): 4489-4495.
15. XUEGUI S, XUANMIN S, HONGHU Y, et al. Stability control of the roadway groupunder the influence of overlying goaf. *J. Journal of Mining & Safety Engineering*, 2016, 33(03): 415-422.
16. YIMIN S, TENGTENG W, DONG A, et al. Simulation test and numerical analysis of the performance of hydraulic support for pile foundation. *J. Coal science and Technology*: 1-11.
17. XIONG Y, KONG D, CHENG Z, et al. Instability control of roadway surrounding rock in close-distance coal seam groups under repeated mining. *J. Energies*, 2021, 14(16): 5193.
18. FENGFENG W, HAOYUAN G, PEIJU Y, et al. Control technology and application of variable-diameter zoned pressure relief forsurrounding rock in deep soft rock and large deformation roadway. *J. Coal Science and Technology*, 2025, 53(02): 53-67.
19. ZHENGIAN M, YAODONG J, YINGMING Y, et al. Floor roadway stabiltyin repeated mining of closedistance coal seams in luling coal mine. *J. Chinese Journal of Rock Mechanics and Engineering*, 2015, 34(S1): 3320-3327.
20. YU G, XIGUI Z, GANGYE G, et al. Study on deformation failure and control of surrounding rock insoft rock roadway in close range coal seam with overhead mining. *J. Journal of Mining & Safety Engineering*, 2018, 35(06): 1142-1149.
21. GUO H. Research and application of anti-impact characteristics of unit type roadway hydraulic support. *D. Liaoning Technical University*, 2024.
22. YIMIN S, XIAODONG J, HAILIANG X, et al. Multi-row telescopic pile foundation three-hinged arch support structure, CN119466891A [P/OL].

Funding

National Major Scientific Instruments and Equipments Development Project of National Natural Science Foundation of China :52427805.

Author Contributions

L.Y. Gou for writing the article, D. An and Y.M. Song for conceptualization, H.L. Xu and W.J. Xiao for methodology, X.D. Jiang for validation, L.Y. Gou for graphic editing, and D. An for visualization and review, the authors have read and agree with the published paper. All authors have read and agreed to the published version of the manuscript.

Additional Information

Competing financial interests: The authors declare no competing financial interests.

Disclaimer/Publisher's Note: The content written is authentic and reliable, all the content is written by ourselves. All statements, opinions and data in the publication represent the personal views of the authors and contributors only and are not related to the editor. The editor is not responsible for any damage to persons or property resulting from any opinions, methods, instructions or products mentioned in the contents.